*Acta Oceanol. Sin.*, 2017, Vol. 36, No. 7, P. 32–38
DOI: 10.1007/s13131-017-1080-5
http://www.hyxb.org.cn
E-mail: hyxbe@263.net

# Sea surface wind speed retrieval under rain with the HY-2 microwave radiometer

WANG Jin[1]*, ZHANG Jie[2], WANG Jing[3]

[1] College of Physics, Qingdao University, Qingdao 266071, China

[2] The First Institute of Oceanography, State Oceanic Administration, Qingdao 266061, China

[3] College of Information Science and Engineering, Ocean University of China, Qingdao 266100, China

Received 30 March 2016; accepted 5 September 2016



**Abstract**

As rain drops change the radiation and scattering characteristic of the oceans and the atmosphere, the wind speed measuring by spaceborne remote sensors under rainy conditions remains challenging for years. On the basis of a microwave radiometer (RM) loaded on HY-2 satellite, the sensitivity of some brightness temperature (TB) channels to a rain rate and the wind speed are analyzed. Consequently, two TB combinations which show minor sensitivity to rain are obtained. Meanwhile, the sensitivity of the TB combination to the wind speed is even better to the original TB channel. On the basis of these TB combinations, a wind speed retrieval algorithm is developed and compared with WindSat all-weather wind speed product, HY-2 RM original wind speed product and buoy *in situ* data. The wind speed retrieval accuracy is better than 2 m/s for rainy conditions, which is evidently superior to HY-2 RM original product. The applicability of this new algorithm is testified for the wind speed measuring in rainy weather with HY-2 RM.

**Key words:** HY-2 microwave radiometer, rain, wind speed, retrieval algorithm, brightness temperature

**Citation:** Wang Jin, Zhang Jie, Wang Jing. 2017. Sea surface wind speed retrieval under rain with the HY-2 microwave radiometer. Acta Oceanologica Sinica, 36(7): 32–38, doi: 10.1007/s13131-017-1080-5

## 1 Introduction

HY-2 is the first satellite mission for the dynamic environmental parameters measurements of China which has been launched successfully on August 16, 2011(Jiang et al., 2013). A multi bands scanning microwave radiometer (RM) is one of the key sensors onboard HY-2 satellite with the primary objective of measuring SST, surface wind speed, water vapor and cloud liquid content. Since the launch of HY-2 in 2011, numerous researchers have discussed the wind speed algorithm and its performance and they argue that the accuracy of HY-2 wind speed product is better than 2 m/s (Jiang et al., 2012; Huang et al., 2014; Wang et al., 2013). It is worth to note that Wang et al. (2014) developed a physical retrieval algorithm for HY-2 RM for both no raining and rainy conditions and the accuracy of wind speed measuring is found to be 1.89 m/s compared with WindSat wind product of 6 months.

In fact, wind speed remote sensing under rain remains challenging for years (Weissman et al., 2012). The signal of active sensors such as scatterometer tends to saturate under a high wind speed and it restricts the application of active sensors to measure a surface wind in severe weather. The microwave radiometer data, nevertheless, are not saturate and even more sensitive to a surface roughness for the high wind speed (Meissner and Wentz, 2012).

Consequently, the microwave radiometers, especially the airborne ones such as hurricane imaging radiometer (HIRAD) and stepped frequency microwave radiometer (SFMR), play an important role in the wind speed measuring in the severe weather, for instance, the hurricanes (Jones et al., 1981; Amarin et al., 2012). These airborne microwave radiometers operate at several frequencies in a relatively narrow band of 4–7 GHz which implies the responses of TB channels to rain drops are analogous. So it is likely to find the TB combinations which are less sensitive to rain.

With regard to the spaceborne microwave radiometers, the situation is quite different. For the sake of measuring various oceanic and atmospheric parameters, the spaceborne radiometers usually work at separated bands which make it hard to employ the algorithm of airborne microwave radiometers to the spaceborne ones. Furthermore, rain drops increase the atmosphere opacity and make it more difficult for the spaceborne microwave radiometer to "see" the sea surface roughness, i.e., the surface wind. Modeling the TB under rainy conditions is hardly possible because some necessary rain parameters are usually unavailable. Consequently, algorithms for the wind speed retrieval under rain are statistical and aim at specific microwave radiometers. The scientific community has develop various algorithms for the wind speed retrieval under rain based on sensitive analyses, rain signal correction and using lower TB band such as 1.4 GHz (Wentz and Spencer, 1998; Adams et al., 2006; Meissner and Wentz, 2009; Reul et al., 2012; Wang et al., 2015). It is worth noted that an all-weather wind speed algorithm established by Meissner and Wentz (2009) has been applied to the latest versions of WindSat geophysical parameter product.

This article focuses on the rainy wind speed algorithm for HY-

Foundation item: The National Science Foundation for Young Scientists of China under contract 41306183; the National High Technology Research and Development Program (863 Program) of China under contract Nos 2013AA09A505 and 2013AA122803.
*Corresponding author, E-mail: wangjin@qdu.edu.cn

2 RM, for the fact that little attention has been paid on this topic. The manuscript is presented as follows. Study datasets are described in Section 2. In Section 3, the sensitivity of the TB to rain and the wind speed is discussed to distinguish the response of the TB to the wind speed and rain drops. The new wind speed algorithm is developed and validated in Section 4. And the conclusions are summarized in Section 5.

## 2 Study datasets

### 2.1 *HY-2 RM brightness temperature*

The HY-2 L1b brightness temperature (TB) dataset is provided by the National Satellite Ocean Application Service (NSOAS) the State Oceanic Administration of China and includes more than 5 800 passes of the year 2012. The format of the microwave radiometer data is the hierarchical data file (HDF). The brightness temperature data are filtered by a land-ocean mask to remove the land contamination. The data of all TB channels and the observation time (UTC) have been resampled onto a fixed earth grid of 0.25°×0.25° which is identical to the remote sensing system (RSS) product standard grid.

### 2.2 *WindSat all-weather wind speed product*

WindSat is the first spaceborne full polarimetric microwave radiometer which has worked operationally in orbit for more than 12 a since its launch in January 2003 (Hiburn et al., 2016). The WindSat data used in this article are the latest version (V7.01) product processed by the RSS which involved an all-weather wind speed algorithm to improve the wind measurement under the rainy conditions.

### 2.3 *HY-2 RM L2 products*

The L2 standard geophysical parameter products of HY-2 RM are obtained from the NSOAS. The wind speed data are checked according a product quality flag and resampled onto the same 0.25°×0.25° grid as the brightness temperature data. Former research has indicated that the accuracy of HY-2 RM wind data was about 1.5 m/s in rain-free weather (Zhou et al., 2013).

### 2.4 *Buoy in situ data*

The *in situ* data from the National Data Buoy Center (NDBC) are filtered as the wind speed and the rain rate can be measured simultaneously. Consequently, there are 22 TAO buoys, 19 RAMA buoys and 15 PIRATA buoys included in this research. The temporal resolution of the buoy measurements varied from 10 min to 1 h. The spatial distributions of buoys are shown in Fig. 1.

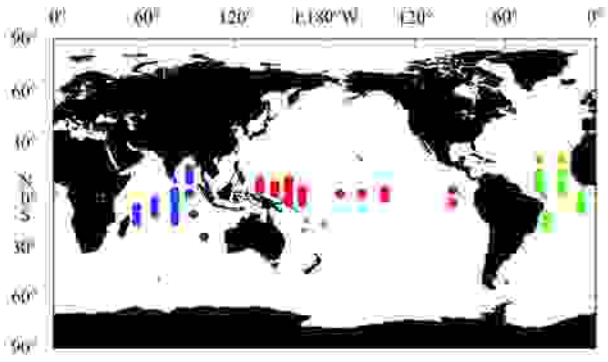

**Fig. 1.** Spatial distributions of buoys. Red represents TAO, green PIRATA, and blue RAMA.

### 2.5 *ECMWF SST reanalysis product*

The primary objective of involving the SST data in the analysis is to correct the effect of the SST imposed to the TB. The SST reanalysis product is provided by the ECMWF (European Centre for Medium-Range Weather Forecasts), which assimilated observations from ships, buoys, and satellites and models. The ECMWF processes the reanalysis product every 6 h (0 UTC, 6 UTC, 12 UTC, 18 UTC) with the spatial resolution of 0.25°.

### 2.6 *Datasets match-up*

In this section, three match-up datasets are collocated for the development and validation of the wind speed algorithm.

For Dataset 1, we collocate the HY-2 brightness temperature with WindSat all-weather wind speed and rain rate data with a spatial and temporal interval of 0.25° and 1 h. All rain-free data are excluded since the objective of this research is to develop a wind speed algorithm under rainy conditions. Because HY-2 and WindSat share approximately the same descending node times (≈06:00 local time) and orbit incline angle (≈99°), this choice guarantees a global coverage of match-up data. Consequently, the amount of the match-up data is more than $7\times10^6$. Dataset 1 is divided into training data and validation data as the radio of 1:9.

For Dataset 2, in order to validate the performance of HY-2 original wind speed data under the rainy conditions, we also collocate HY-2 Level 2 wind speed product with WindSat all-weather wind speed and rain rate data with the same spatial and temporal interval as the former paragraph. The final match-up data are more than $10^7$.

For Dataset 3, this dataset consists of the HY-2 RM brightness temperature, the HY-2 original wind speed, and *in situ* wind speed of TAO, RAMA and PIRATA buoys. Because of the relatively high frequency of buoy measurements, the temporal interval is set to be 10 min, and the spatial interval is 0.25°. Consequently, we get 3 599 match-up data for the HY-2 brightness temperature and buoy data, and 5 447 match-up data for the HY-2 original wind speed and buoy data.

## 3 Dependence of TB on geophysical parameters

### 3.1 *TB dependence on SST*

Theoretical studies have proved that the brightness temperature channel higher than 10 GHz is sensitive to the sea surface roughness and the atmosphere conditions (Martin, 2004; Ulaby and Long, 2014). These high frequency channels are the primary channels for the remote sensing of the wind speed, the water vapor content and the cloud liquid water content. When it is raining, the rain drops will mask the ocean surface, change the roughness of the ocean surface, and combine the radiation of the ocean surface and the precipitating atmosphere. As a result, the wind speed algorithms using high frequency TB channels become invalid under rain. In contrary to high frequency channels, the fact that the C/X band TB (6.6 and 10.7 GHz of HY-2 RM) is less sensitive to an atmosphere parameter, make it feasible to measure the wind speed with some specific combination of brightness temperature channels under rain. It is worth noted that the principal purpose of a low frequency is to measure the SST and the maximum sensitivity of these channels to the SST is 0.5 (6.6 GHz, V polarization, 50° incidence angel). Therefore, the effect of the SST-induced on the TB becomes a fake signal in the case of wind speed measurement, and need to be removed.

To correct the SST effect, ECMWF reanalysis SST data are interpolated linearly to the observation locations of the HY-2 RM. The SST data of the HY-2 RM is not involved in this process for the consideration of data independence. The radiations of the flat

sea surface are calculated based on a dielectric constant model of sea water (Klein and Swift, 1977). Then the calculation results are subtracted from the HY-2 RM observed TB data as

$$\Delta T_{\mathrm{b,\,rp}} = T_{\mathrm{b,\,ob}} - T_{\mathrm{b,\,fss}}, \tag{1}$$

where the $T_{\mathrm{b,\,ob}}$ is the HY-2 observed TB, $T_{\mathrm{b,\,fss}}$ is the radiation of the flat sea surface calculated by Klein model, and $\Delta T_{\mathrm{b,\,rp}}$ is the residual part of the TB.

To investigate the independence of the residual TB to SST, the residual TB and original TB data of C/X band are compared in an SST range of 270–305 K. It is noted that all original TB data are subtracted a constant to display these data and residual TB in the same figure. As shown in Fig. 2, the SST-induced signal in the residual TB (blue line) is less than 5 K for 6 H/V and 10 V band which is about four times less than the original TB (red line).

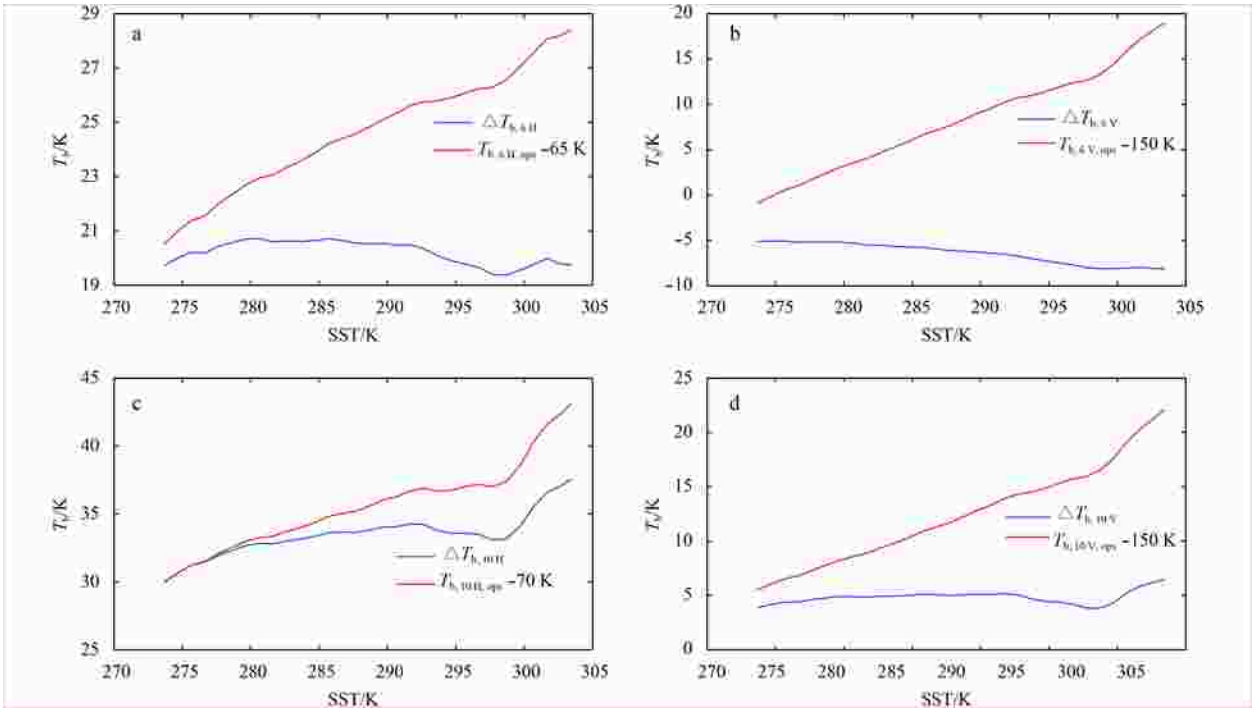


**Fig. 2.** Comparison of residual TB (blue line) and original TB data (red line). a. 6.6 H, b. 6.6 V, c. 10.7 H, and d. 10.7 V.

### 3.2 *TB dependence on rain rate*

The sensitivity ($S_{T_b}$, $r_{\mathrm{r}}$)of the TB to the rain rate is defined as

$$s_{T_{\mathrm{b}},\,r_{\mathrm{r}}} = \frac{\partial T_{\mathrm{b}}}{\partial r}, \tag{2}$$

which is the slope of the curve of the TB and rain rate ($r$).

For a channel combination that has minimal sensitivity to precipitating, it means

$$\frac{\partial (T_{\mathrm{b1}} - \lambda T_{\mathrm{b2}})}{\partial r} = 0 \quad \text{or} \quad \lambda = \frac{\partial T_{\mathrm{b1}}/\partial r}{\partial T_{\mathrm{b2}}/\partial r}. \tag{3}$$

Equation (3) shows that the parameter $\lambda$ equals the sensitivity ratio of the TB channels. In the work of Meissner and Wentz (2009), the parameter $\lambda$ is defined as the sensitivity ratio of transmittance $\tau^2$. Since it is the TB but not the transmittance is the input parameter for the wind speed retrieval algorithm, we believe the definition of the parameter $\lambda$ in this research is straighter.

To investigate the sensitivity of the TB channels to the rain rate, the curves of different TB channels and rain rates are plotted in Fig. 3 within a rain rate range of 0.5–20 mm/h with an increment of 0.5 mm/h.

It is obvious that the brightness temperatures increase to a maximum at the rain rate of 12 mm/h, and then decrease slightly

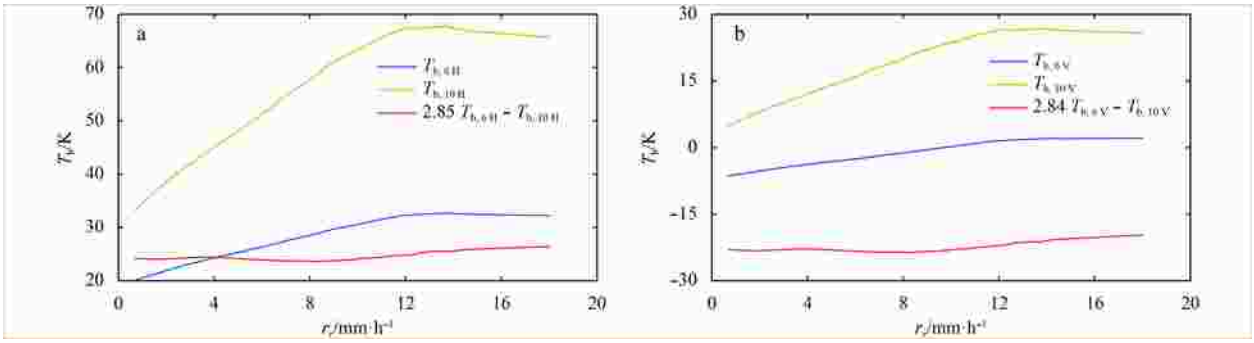


**Fig. 3.** The dependence of the TB to the rain rate. a. H-pol and b. V-pol.

as the rain rate increases. This dependence of the TB to the rain rate has been confirmed by some former research (Zabolotskikh et al., 2015; Wentz, 1983). It is worth noted that the minimal sensitivity that the TB combinations (red line in Fig. 3) with the rain rate indicates the possibility for the wind speed measuring with these TB combinations under rain. The sensitivities of different TB channels to the rain rate are studied in Table 1. The sensitivities of the channel combinations drop off dramatically.

**Table 1.** The sensitivities of the TB channels to the rain rate

| Channel | Sensitivity/ K·mm$^{-1}$·h | Channel | Sensitivity/ K·mm$^{-1}$·h |
|---|---|---|---|
| 6 H | 1.15 | 6 V | 0.72 |
| 10 H | 3.29 | 10 V | 2.05 |
| 2.85 by 6–10 H | 0.086 | 2.84 by 6–10 V | 0.074 |

### 3.3 *TB dependence on wind speed*

The dependence of the sensitivity of the TB combinations on wind speed is shown in Fig. 4 and Table 2. The wind speed range is 2 to 25 m/s with an increment of 1 m/s. The TB combinations show better sensitivity to the wind speed than the original TB channels of 6 GH and 10 GHz. As the sensitivity is the primary consideration for measuring geophysical parameter with some TB channels, this result is quite encouraging.

## 4 Development and validation of all-weather wind speed algorithm

### 4.1 *Wind speed algorithm based on neural network*

Dataset 1 described in Section 2.6 is divided into two datasets randomly for an algorithm development and validation. The dataset for the algorithm development contains 10% of all data. As the dependence of the TB on the wind speed is nonlinear, the wind speed algorithm is developed based on a neural network (NN) method. The neural network is a two-layers feed forward model which consists of a single hidden layer with ten neurons and an output layer with one neuron. The transfer functions of the hidden and output layers are sigmoid and linear function. The training function is the Levenberg-Marquardt method. The input of the NN is the C/X band TB combinations obtained in Section 3.2 and the output is the wind speed.

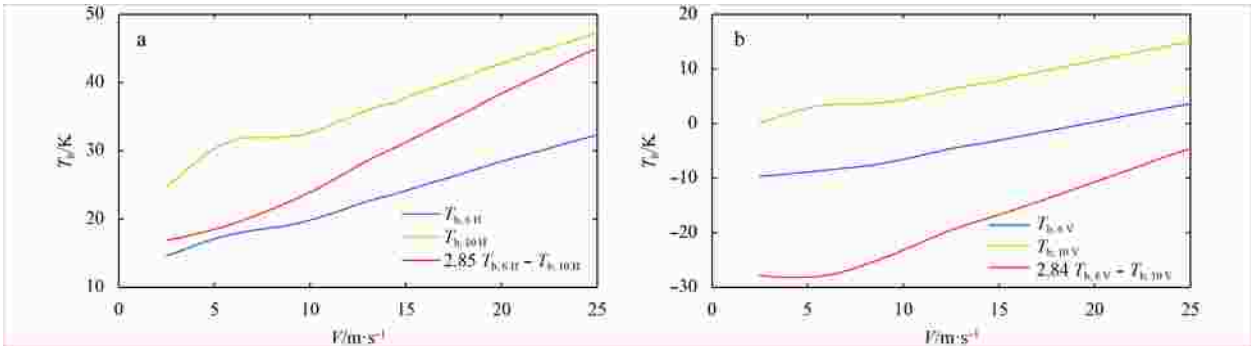


**Fig. 4.** The dependence of the TB on wind speed $V$. a. H-pol and b. V-pol.

**Table 2.** The sensitivities of the TB channels to the wind speed

| Channel | Sensitivity/K·m$^{-1}$·s | Channel | Sensitivity/K·m$^{-1}$·s |
|---|---|---|---|
| 6 H | 0.76 | 6 V | 0.59 |
| 10 H | 0.87 | 10 V | 0.59 |
| 2.85 by 6–10 H | 1.28 | 2.84 by 6–10 V | 1.11 |

The wind speed retrieving by our new algorithm in an actual rain band is studied and compared with the HY-2 RM and the WindSat product. The study area is the north Pacific (10°–60°N, 120°–220°E). The data involved in this part are the descending passes of HY-2 RM and WindSat on the date of October 29, 2012. As is discussed in Section 2.6, WindSat shares orbit parameters with HY-2 RM, so these two radiometers have the approximate spatial coverage.

It is obvious that the HY-2 RM wind speed is higher than 30 m/s in three rainy areas (red box in Fig. 5b). According to the all-weather wind speed product of WindSat (Fig. 5c), the wind speed in these areas is lower than 15 m/s, but the precipitation is very severe (Fig. 5d). The similar spatial patterns of the HY-2 RM product and the WindSat rain rate prove that the original HY-2 RM product maps the rain rate rather than the wind speed and results in false wind speed data in rain bands. In contrast, the new algorithm distinguishes the signal of the wind speed from rain drops clearly. There is no false wind speed in rainy bands and the spatial pattern of the new algorithm is similar to the WindSat all-weather wind speed product.

### 4.2 *Comparison with WindSat all-weather wind speed*

In this section, the results of the new wind speed algorithm are compared with the WindSat all-weather wind speed data in rainy conditions. A bias and a standard deviation are obtained to evaluate the performance of algorithm. Meanwhile, to discover the improvement of our new algorithm, the quality of the original HY-2 RM wind speed products is also validated by the WindSat data. Figure 6 shows the scatter plot of the new algorithm and the HY-2 original product. It is obvious that the result of our new algorithm is fairly superior to the HY-2 RM product. The HY-2 RM data deviate from the 1:1 line even if the wind speed is above 5 m/s. In the contrary, the new algorithm shows no explicit deviation within the total range of the wind speed.

The statistics of the new algorithm and the HY-2 original product are summarized in Table 3. Our new algorithm shows a tiny systematic error of –0.17 m/s. However the HY-2 RM product has a large bias more than 1 m/s. The random error of the new algorithm is better than 2 m/s achieving the performance of the wind speed measurement under no rain conditions. At the same time, the standard deviation of the HY-2 RM product is as big as 3.22 m/s.

### 4.3 *Validation by buoy in situ data*

In this section, our new algorithm is validated by the *in situ* data of TAO, RAMA and PIRATA buoy. The rain-free data are filtered by the rain rate measured by buoys. Because the typical

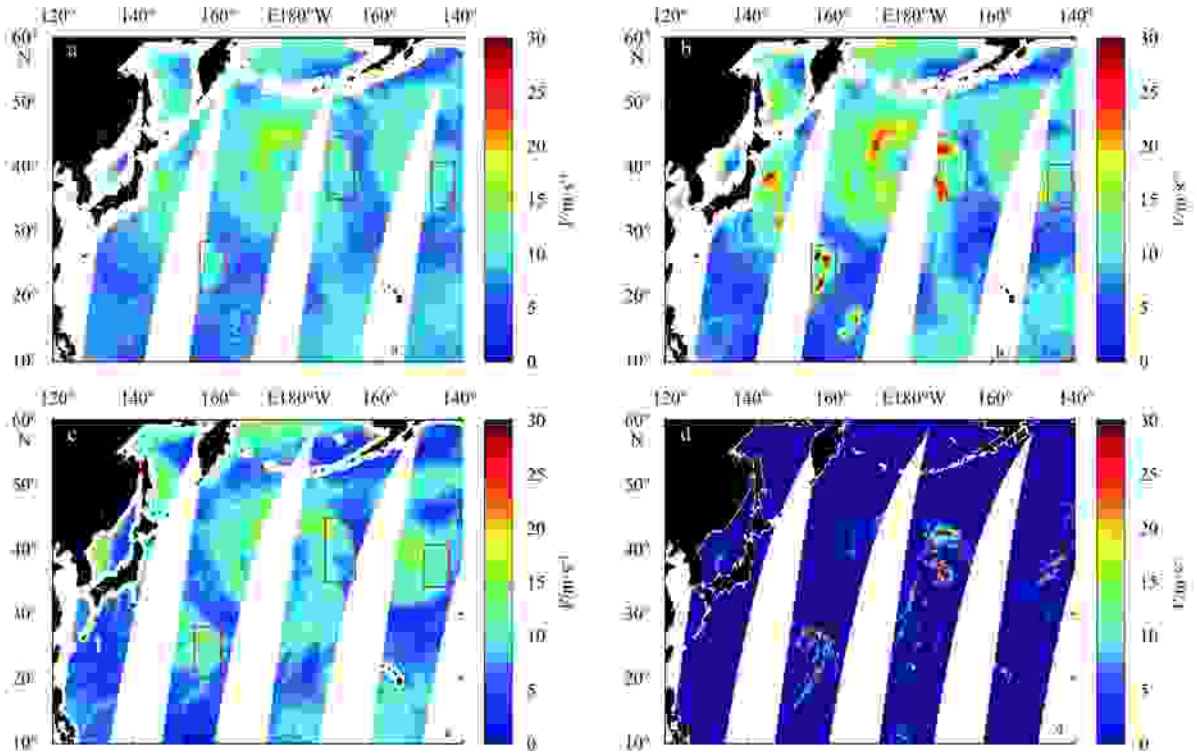

**Fig. 5.** The wind speed of the new algorithm (a), Y-2 original product (b), WindSat all-weather wind speed (c), and WindSat rain rate (d).

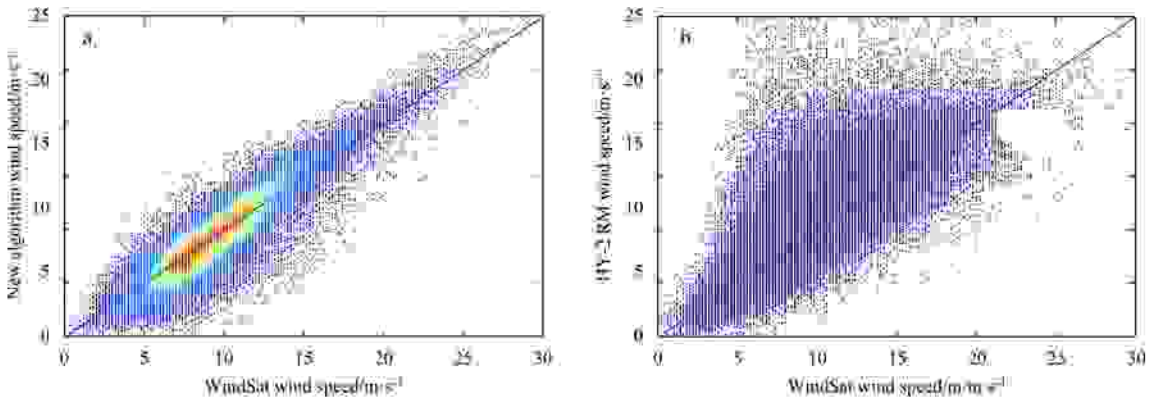

**Fig. 6.** Scatter diagram of new algorithm (a) and HY-2 RM original product (b).

**Table 3.** Statistics of the new algorithm and the HY-2 original product

| Statistics | New algorithm | HY-2 product |
|---|---|---|
| Bias/m·s$^{-1}$ | –0.17 | 1.26 |
| Standard deviation/m·s$^{-1}$ | 1.73 | 3.22 |
| Correlation coefficient | 0.91 | 0.72 |

height of an anemometer is 4 m and the microwave radiometer measures the wind speed ($U_{10}$) at 10 m above the sea surface, the 4 m *in situ* wind speed is converted to 10 m by a logarithmic wind profile (Wentz, 1997):

$$\frac{U_{10}}{U_H} = \frac{\ln(10/z_0)}{\ln(H/z_0)}, \tag{4}$$

where $H$ is the anemometer height onboard buoys and $z_0$ is the surface roughness length $1.52\times10^{-4}$ m.

The statistic results are shown in Tables 4 and 5. As is expected, the result of the new algorithm is evidently superior to the HY-2 RM product for all three buoy systems. It is worth noted that the accuracy of the new algorithm shows no sensitivity to the rain rate. The data of the TAO buoy have the maximum mean rain rate of 0.46 mm/h, which is two times bigger than the PIRATA buoy. However the error of the new algorithm is quite steady. Instead, the HY-2 RM products show highly sensitive to rain. For the most precipitation region of the TAO buoy, the sys-

**Table 4.** Statistics of new algorithm compared with buoy data

| Buoy | Data amount | Mean rain rate/mm· h$^{-1}$ | Mean bias/m·s$^{-1}$ | Standard deviation/m·s$^{-1}$ |
|---|---|---|---|---|
| TAO | 1 116 | 0.46 | –0.06 | 1.37 |
| RAMA | 1 091 | 0.36 | 0.19 | 1.74 |
| PIRATA | 1 392 | 0.20 | 0.05 | 1.51 |
| All data | 3 599 | 0.33 | 0.07 | 1.57 |

**Table 5.** Statistics of HY-2 product compared with buoy data

| Buoy | Data amount | Mean rain rate/mm·h$^{-1}$ | Mean bias/m·s$^{-1}$ | Standard deviation/m·s$^{-1}$ |
|---|---|---|---|---|
| TAO | 1 359 | 0.58 | 1.18 | 3.19 |
| RAMA | 1 388 | 0.39 | 0.89 | 2.78 |
| PIRATA | 2 700 | 0.19 | 0.26 | 2.10 |
| All data | 5 447 | 0.34 | 0.65 | 2.61 |

tematic and random errors of the HY-2 RM are biggest. And for the region of the PIRATA buoy with the minimum precipitation, the HY-2 product shows the minimum error. It is evident that the performance of the original algorithm of HY-2 RM which is trained for no rain conditions, decrease dramatically under rain. The detailed results will be described in the following section.

### 4.4 *Dependence of retrieval error on rain rate*

The accuracy of the new algorithm and the HY-2 RM product is estimated with a rain rate range of 0–20 mm/h with an increment of 2 mm/h in Fig. 7. The new algorithm shows no systemic error and the random error is better than 2 m/s when the rain rate is less than 4 mm/h which covers 95% of the match-up data. The bias becomes higher as the rain rate increases which reaches the maximum value of –1 m/s at the rain rate of 12 mm/h. The standard deviation increases as the rain rate rises, but it is no more than 3 m/s in all circumstances.

The performance of the HY-2 RM product is quite different to the new algorithm. The bias of the HY-2 wind speed product increases by 1m/s as the rain rate enlarges by 1 mm/h within a rain rate range of 0–13 mm/h. When the rain rate is higher than 13 mm/h, the mean bias decreases with the rain rate rises, but remains above 10 m/s. The standard deviation of the HY-2 RM is about 3 m/s for all rain rate conditions. The characteristic of the standard deviation is somewhat similar to the bias, which increases quickly as the rain rate rises and reaches the maximum value of 8.1 m/s at the rain rate of 14 mm/h.

### 4.5 *Dependence of retrieval error on wind speed*

The error of the new algorithm and the HY-2 RM product is studied under the wind speed range of 0–30 m/s with an increment of 2 m/s. The mean bias of our new algorithm is better than 0.5 m/s. The standard deviation is better than 2 m/s if the wind speed is less than 15 m/s and increases to the maximum value of 2.8 m/s as the wind speed rises. The HY-2 RM product has a positive bias of 0.4–1.7 m/s with the wind speed range of 0–17 m/s, and it decreases to –4.3 m/s when the wind speed increases. The standard derivation of the HY-2 RM is more than 3 m/s if the wind speed is above 5 m/s, which covers 98% of data amount.

## 5 Conclusions

In this research, a new wind speed algorithm for rainy atmo-

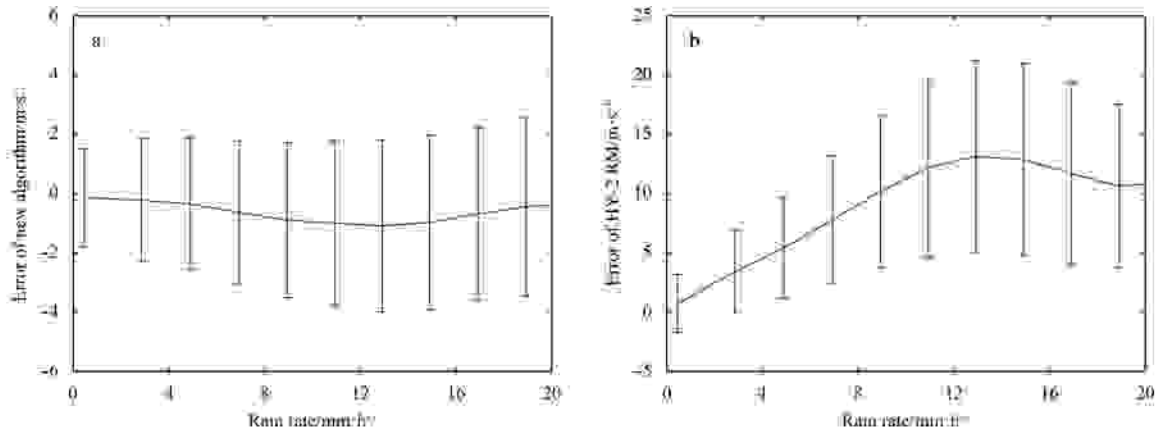


**Fig. 7.** Mean value of error±1 standard deviation as function of rain rate. a. New algorithm and b. HY-2 original product.

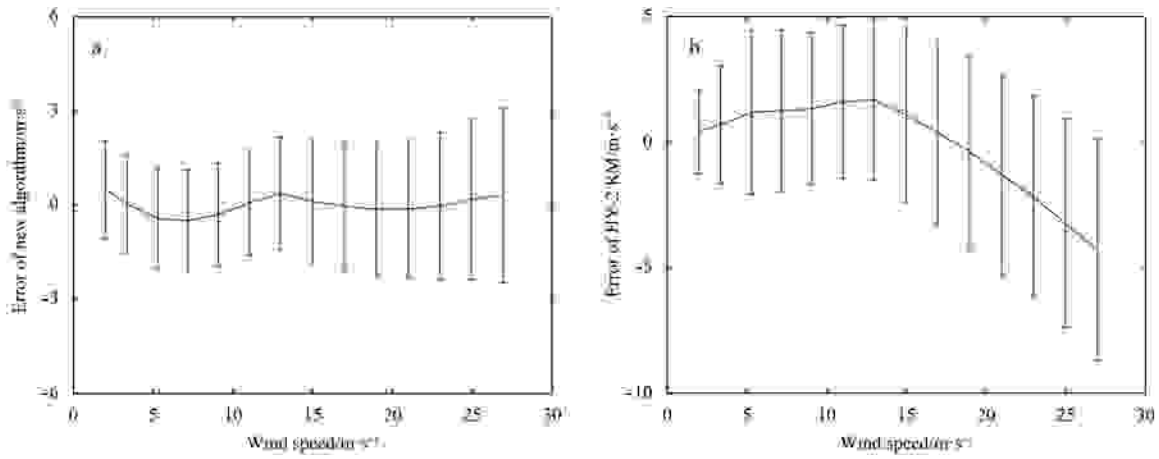


**Fig. 8.** Mean value of error plus or minus one standard deviation as function of the wind speed. a. New algorithm and b. HY-2 original product.

sphere based on the HY-2 microwave radiometer is developed and validated. The sensitivity of the C/X band brightness temperature to the rain and the wind speed is discussed and two TB combinations that are insensitive to rain rate are obtained. The sensitivity of the TB combination is less than 0.1 K/(mm·h$^{-1}$), which is two-three orders of magnitude lower than the original TB band. Furthermore, the sensitivity of the TB combination to the wind speed is two times as high as the original TB band. Consequently, a new wind speed algorithm is founded base on a neural network. An example of the wind speed retrieval in actual rain bonds is provided which verifies the applicability of applying the algorithm as a rainy weather wind speed algorithm. The error characteristic of this algorithm is studied by comparing with the WindSat all-weather product, the HY-2 RM original product and the buoy *in situ* measurements in rainy situations. The error analysis indicates that the new algorithm achieves the accuracy better than 2 m/s which means an definite improvement in the wind speed remote sensing for the HY-2 RM.

***Acknowledgements***

The authors thank the National Ocean Satellite Application Center, State Oceanic Administration, Remote Sensing Systems, NDBC, ECMWF for providing access to data involved in the research.

**References**

Adams I S, Hennon C C, Jones W L, et al. 2006. Evaluation of hurricane ocean vector winds from WindSat. IEEE Trans Geosci Remote Sens, 44(3): 656–667

Amarin R A, Jones W L, El-Nimri S F, et al. 2012. Hurricane wind speed measurements in rainy c onditions using the airborne hurricane imaging radiometer (HIRAD). IEEE Trans Geosci Remote Sens, 50(1): 180–192

Hiburn K A, Meissner T, Wentz F J, et al. 2016. Ocean vector winds from WindSat two-look polarimetric radiances. IEEE Trans Geosci Remote Sens, 54(2): 918–931

Huang Xiaoqi, Zhu Jianhua, Lin Mingsen, et al. 2014. A preliminary assessment of the sea surface wind speed production of HY-2 scanning microwave radiometer. Acta Oceanologica Sinica, 33(1): 114–119

Jiang Xingwei, Lin Mingsen, Liu Jianqiang, et al. 2012. The HY-2 satellite and its preliminary assessment. Int J Digit Earth, 5(3): 266–281

Jiang Xingwei, Lin Mingsen, Song Qingtao. 2013. Active and passive microwave remote sensing technology of the HY-2A ocean satellite mission. Eng Sci (in Chinese), 15(7): 4–11

Jones W L, Swift C T, Black P G, et al. 1981. Airborne microwave remote-sensing measurements of Hurricane Allen. Science, 214(4518): 274–280

Klein L, Swift C. 1977. An improved model for the dielectric constant of sea water at microwave frequencies. IEEE Trans Antennas Propag, 25(1): 104–111

Martin S. 2004. An Introduction to Ocean Remote Sensing. Cambridge: Cambridge University Press, 237–238

Meissner T, Wentz F J. 2009. Wind-vector retrievals under rain with passive satellite microwave radiometers. IEEE Trans Geosci Remote Sens, 47(9): 3065–3083

Meissner T, Wentz F J. 2012. The emissivity of the ocean surface between 6 and 90 GHz over a large range of wind speeds and earth incidence angles. IEEE Trans Geosci Remote Sens, 50(8): 3004–3026

Reul N, Tenerelli J, Chapron B, et al. 2012. SMOS satellite L-band radiometer: a new capability for ocean surface remote sensing in hurricanes. J Geophys Res, 117(C2): doi: 10.1029/2011JC007474

Ulaby F, Long D G. 2014. Microwave Radar and Radiometric Remote Sensing. Michigan, US: The University of Michigan Press, 896–897

Wang Zhenzhan, Bao Jinghua, Li Yun, et al. 2014. Study on retrieval algorithm of ocean parameters for the HY-2 scanning microwave radiometer. Eng Sci (in Chinese), 16(6): 70–82

Wang Jin, Zhang Jie, Fan Chenqing, et al. 2015. A new algorithm for sea-surface wind-speed retrieval based on the L-band radiometer onboard Aquarius. Chin J Oceanol Limnol, 33(5): 1115–1123

Wang He, Zhu Jianhua, Lin Mingsen, et al. 2013. First six months quality assessment of HY-2A SCAT wind products using in situ measurements. Acta Oceanologica Sinica, 32(11): 27–33

Weissman D E, Stiles B W, Hristova-veleva S M, et al. 2012. Challenges to satellite sensors of ocean winds: addressing precipitation effects. J Atmos Oceanic Technol, 29(3): 356–374

Wentz F J. 1983. A model function for ocean microwave brightness temperatures. J Geophys Res, 88(C3): 1892–1908

Wentz F J. 1997. A well-calibrated ocean algorithm for special sensor microwave/imager. J Geophys Res, 102(C4): 8703–8718

Wentz F J, Spencer R W. 1998. SSM/I rain retrievals within a unified all-weather ocean algorithm. J Atmos Sci, 55(9): 1613–1627

Zabolotskikh E, Mitnik L, Reul N, et al. 2015. New possibilities for geophysical parameter retrievals opened by GCOM-W1 AMSR2. IEEE J Sel Top Appl Earth Obs Remote Sens, 8(9): 4248–4261

Zhou Wu, Lin Mingsen, Li Yanmin, et al. 2013. Study of cold sky calibration and geophysical parameters retrieval for HY-2A satellite scanning microwave radiometer. Eng Sci (in Chinese), 15(7): 75–80